ORCA – Online Research @ Cardiff

# Seed- and Solvent-Free Synthesis of ZSM-5 with Tuneable Si/Al Ratios for Biomass Hydrogenation

Bin Zhang[†,‡,§], Mark Douthwaite[§], Qiang Liu[†], Chao Zhang[†,*], Qifan Wu[†], Ruhui Shi[†], Peixuan Wu[†], Ke Liu[†], Zhuangqing Wang[†], Weiwei Lin[†], Haiyang Cheng[†], Ding Ma[‡], Fengyu Zhao[†], Graham J. Hutchings[§,*]

† State Key Laboratory of Electroanalytical Chemistry and Laboratory of Green Chemistry and Process, Changchun Institute of Applied Chemistry, Chinese Academy of Sciences, Changchun 130022, China

‡ Beijing National Laboratory for Molecular Sciences, College of Chemistry and Molecular Engineering and College of Engineering, and BIC-ESAT, Peking University, Beijing 100871, China.

§ Cardiff Catalysis Institute, School of Chemistry, Cardiff University, Cardiff, CF10 3AT, UK

ABSTRACT: A novel method for the synthesis of MFI zeolites has been developed, which does not require any crystal seeds or solvent. The adaptability of this method was also evidenced; a series of ZSM-5 zeolites with differing Si/Al ratios (18~∞) were synthesized, which to date, has been a challenge in the field of solvent-free synthesis. The materials were probed by in-situ DRIFTS and 2D ^{27}Al-^{19}F HETCOR NMR spectroscopy, the results from which indicated that fluorine-containing species play a crucial role in the crystallization of ZSM-5. During the crystallization process F$^-$ anions coordinate with Al^{3+} cations, resulting in the formation of 6-coordinated "F-Al-O-Si" species. It is these intermediate species which drive the formation of tetrahedral [AlO$_4$]$^-$ units in the zeolitic framework. The effectiveness of these materials as catalyst supports was subsequently assessed in the hydrogenation of levulinic acid and glucose, which exhibited a comparable performance to commercial ZSM-5. The simple, efficient and low-cost method presented herein provides an alternative approach for the green scaled-up synthesis of zeolites.
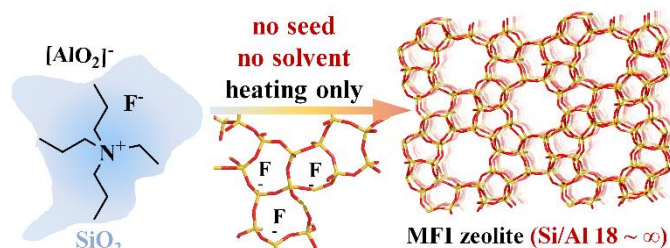
KEYWORDS: *Seed-free synthesis; solvent-free synthesis; ZSM-5 zeolite; solid-phase crystallization; biomass hydrogenation*

INTRODUCTION

Zeolite Socony Mobil-5 (ZSM-5) is a crystalline aluminosilicate zeolite with an MFI framework. It is one of the most commonly used catalysts in the petrochemical and fine chemical industries and has recently displayed promise in the field of biomass valorization, by virtue of its strong acidic sites and structural geometry.[1, 2] ZSM-5 was first synthesized in 1969 by Argauer and Landolt [3] using a hydrothermal method. This was soon followed by the development of other synthetic methodologies, such as solvothermal and ionothermal routes.[4-6] These methods are usually conducted in sealed autoclaves with large amounts of solvent, which inevitably leads to the accumulation of large amounts of waste. Furthermore, the use of a solvent can result in the dissolution and loss of silica-based species in the alkaline media, and results in synthesis occurring under high autogenous pressure.[7] To overcome these limitations, dry gel and vapor-phase transfer methods were developed.[8-10] While both of these approaches have been confirmed as effective methods for the synthesis of zeolites, large amounts of water are still required as a solvent to prepare the starting precursor.

In 2012, Xiao and co-workers developed a novel synthetic methodology for the solvent-free synthesis of zeolitic materials.[11, 12] An all-silica MFI zeolite was obtained simply by mixing and heating raw materials: SiO$_2$ gel, sodium silicate hydrate, tetrapropylammonium bromide, and NH$_4$Cl.[13, 14] It was also demonstrated that the aluminosilicate ZSM-5 (with a Si/Al ratio of 14.3) could also be produced in this way, when zeolite seeds were incorporated into the preparative procedure; these seeds are considered to be essential for the formation of the zeolites. Despite this innovative development, dense phases or MOR impurities were generated concomitantly when the methodology was trialled for the synthesis of ZSM-5. As such, the solvent-free synthesis of ZSM-5 zeolites with wide Si/Al ratios, remains a challenge, particularly in the absence of crystallite seeds.[15]

Understanding the role of F$^-$ anions in the zeolite crystallization process has always been a very significant topic. Since the initial work by Xiao and co-workers, additional zeolites such as MFI,

BEA, EUO and TON have also been synthesized in the presence of NH_4F.[16, 17] The presence of F^- anions was considered to result in the formation of SiF_6^{2-} species, which are suggested to initiate the crystallization of amorphous SiO_2. However, the role of anionic F^- species in the formation of the crystal from this amorphous phase remains elusive.[18]

The work herein, reports on a novel solvent-free and seed-free methodology, that can be used to synthesize MFI zeolites using only two reagents; SiO_2 and $C_{12}H_{28}NF$. It was also established that through combination of these two precursors with $NaAlO_2$, the method could be used to synthesize ZSM-5 materials with Si/Al ratios ranging from 18 to infinity. Various additional Al precursors, $(C_3H_7O)_3Al$, $(C_4H_9O)_3Al$, $AlCl_3$, $(NH_4)_3AlF_6$ and $Al_2(SO_4)_3$, were also investigated and found to significantly influence the ratios of Si/Al in the final ZSM-5. The resultant zeolite herein was probed by a series of analysis techniques (in-situ DRIFTS, 1D $^{19}F/^{27}Al/^{29}Si$ NMR and 2D ^{27}Al-^{19}F HETCOR NMR), the results from which evidenced that F^- anions coordinate with Al^{3+} cations, which results in the formation of 6-coordinated "F-Al-O-Si" species during solvent-free synthesis. This study uncovered the crucial role of F^- and provideed further insights into the mechanism of solid-phase crystallization of ZSM-5.

EXPERIMENTAL SECTION

Materials. Sodium aluminate ($NaAlO_2$, Aladdin), aluminium isopropoxide [$(C_3H_7O)_3Al$, Tokyo Chemical Industry], aluminum sec-butoxide [$(C_4H_9O)_3Al$, Aladdin], aluminum chloride ($AlCl_3 \cdot 6H_2O$, Aladdin), ammonium fluoroaluminate [$(NH_4)_3AlF_6$, Aladdin], tetrapropylammonium fluoride ($C_{12}H_{28}NF \cdot 2H_2O$, J&K Chemical Reagent Co, Ltd.), solid silica gel (Qingdao Haiyang Chemical Reagent Co, Ltd.), commerical zeolite (XFNANO Materials Tech Co, Ltd). All chemicals were used direct without further purification.

Synthesis. In a typical run, 1.6 g silica, 0.3-0.9 g $C_{12}H_{28}NF \cdot 2H_2O$ and a certain amount of Al precursor according to a Si/Al ratio were mixed and ground in a mortar for ten minutes, then transferred to an autoclave and sealed. The autoclave was heated at 180 °C for a given time. Once finished, the sample was cooled down. Then the obtained samples were directly for XRD characterization, the X-ray Fluorescence spectrum and NMR spectrum characterization. And the Si/Al ratio in the feed therefore was adopted in this work. Prior to preparing the zeolite supported Ru catalysts, all the zeolite support are calcined at 550 °C for 4 h in air. Then $RuCl_3 \cdot xH_2O$ as a Ru precursor was loaded on the support in water by the wetness impregnation.

Characterization. The X-ray powder diffraction (XRD) patterns of catalysts were obtained with a Bruker D8 Advance X-ray powder diffraction instrument, using Cu-Ka radiation (k=0.154 nm). Transmission electron microscopy (TEM) images were taken using a field emission JEOL JEM-2010 instrument at 200 kV. N_2 adsorption-desorption experiments (BET) were performed with a Micromeritics ASAP 2020 surface area and porosity analyzer. TGA was conducted in Mettler Toledo. In situ DRIFT experiments were conducted in Thermo Scientific Nicolet Is50. Pyridine-FTIR was conducted in CRCP-7070 platform in Tianjin Xianquan company.

Solid-state NMR experiments were performed on a Bruker AVANCE III 400 MHz spectrometer operating at Larmor frequencies of 399.33, 375.71, 104.06, and 79.33 MHz for the ^1H, ^{19}F, ^{27}Al, and ^{29}Si nucleus, respectively. Solid-state ^{19}F and ^{27}Al NMR spectra were recorded using a 4 mm magic-angle-spinning (MAS) probe operating at a spinning rate of 12.5 kHz. A single-pulse sequence with a $\pi/2$ pulse length of 2.4 µs and a recycle delay of 5 s was used for the ^{19}F NMR experiments, whereas ^{27}Al MAS NMR spectra were recorded using a single-pulse sequence with a pulse length of 1.2 µs ($\pi/2$) and a recycle delay of 1 s. Two-dimensional (2D) ^{19}F-^{27}Al heteronuclear correlation (HETCOR)[1] experiments were carried out with a CP contact time of 4 ms and a recycle delay of 3 s. All 1D ^{29}Si MAS NMR experiments were conducted with high power proton (^1H) decoupling using a $\pi/2$ pulse of 4.9 us and a recycle delay of 80 s on a 7 mm triple-resonance MAS probe with a spinning rate of 5 kHz. The chemical shifts of the ^{19}F, ^{27}Al, and ^{29}Si nucleus were externally referenced to $CFCl_3$, 1 M aqueous $Al(NO_3)_3$, and kaolinite (-91.5 ppm), respectively.

Catalytic tests. In a standard experiment, 4.0 mL of 1.2510 mol/L LA solution together with 20 mg of the reduced catalyst was added into a 30 mL Teflon-lined stainless reactor with a magnetic stirring bar. The reactor was flushed with H_2 for three times and then pressurized with 3.0 MPa H_2 (RT). After a stirred-free preheating for 15 min at 70 °C, the reaction started with stirring of 1300 rpm. After the reaction finished, the reactor was cooled to room temperature and the mixture was centrifuged with water and ethanol, the solid was dried at 70 °C overnight. All remaining filtration was transferred into a volumetric flask, and 1.0 mL 1,3-PDO solution as an internal standard was added before diluting to 50 mL with ethanol. Then the solution was analyzed using a gas chromatograph (Shimadzu, 14C) equipped with a capillary column (RestekStabilwax 30 m×0.53mm×1um) and a flame ionization detector (FID). The hydrogenation reaction procedure of glucose is the same as the hydrogenation of levulinic acid.
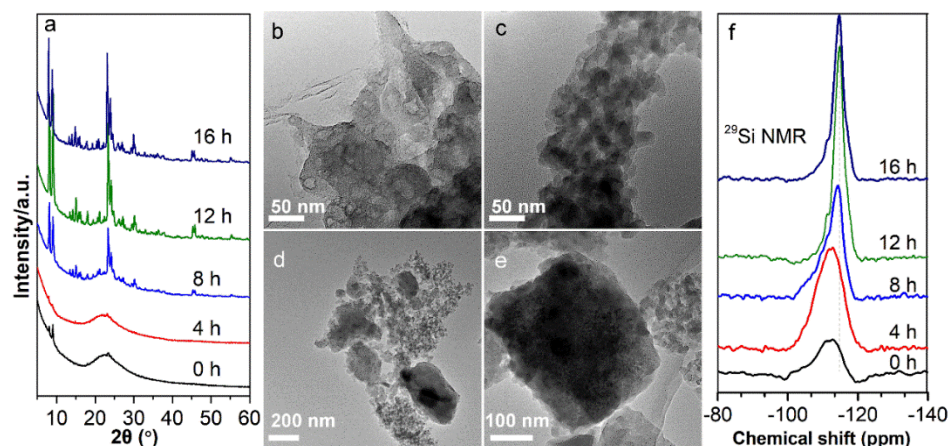
RESULTS AND DISCUSSION

Synthesis of all-silicon MFI zeolite.

Inspired by the work of Xiao and co-workers,[11, 16] we attempted to reproduced the synthesis of the MFI zeolite but substituted the starting materials (SiO_2 gel, sodium silicate hydrate, tetrapropylammonium bromide and NH_4Cl) with SiO_2 and $C_{12}H_{28}NF$. Through trial and error, an effective synthesis procedure was established: a defined amount of SiO_2 and $C_{12}H_{28}NF$ were mechanically ground and sealed for crystallization in an autoclave at 180 °C for 12 h. The crystallization temperature was established to be an important parameter in the formation of the zeolite. When aged at a temperature below 150 °C it was evident that crystalline zeolitic materials could not be obtained, even if the crystallization time was prolonged extensively (Figure S1). However, when an aging temperature in excess of 150 °C was utilized, crystalline zeolitic materials were obtainable. In Figure 1, the diffraction patterns and morphologies of samples synthesized from SiO_2 and $C_{12}H_{28}NF$ after various times of crystallization at 180 °C are displayed. Figure 1a evidences that at 180 °C, the SiO_2 remains amorphous for the first 4 h of the reaction. The characteristic MFI diffraction peaks ($2\theta = 7.8°$, $8.7°$, $22.94°$, $23.6°$, $24.26°$, $45°$) gradually increased with reaction time from 4 to 12 h. No further changes in crystallinity were observed at crystallization time over 16 h. The evolution of the materials is also evidenced by TEM (Figures 1b-1e). The samples transformed from amorphous col-

loidal mixtures (Figure 1b) to colloidal aggregations after 4 h (Figure 1c), and partially crystallized to small fragments after another 4 h (Figure 1d), until the final MFI zeolite was formed at crystallization time of 12 h or longer (Figure 1e). The crystallization process at different stages was also monitored by ^{29}Si NMR measurements (Figure 1f). The resonance at *ca.* -112 ppm is characteristic of the Si(4Si) species[19-22] and evidently becomes more defined and enhanced as the crystallization time is extended, further evidencing that the crystallinity of the material increased over time.

The material recovered after 12 h of crystallization was subsequently probed by N_2 sorption. This material exhibited a BET surface area and pore volume of 212 m^2/g and 0.31 cm^3/g, respectively (Figure S2), which was comparable to the hydrothermally prepared commercial MFI zeolite (256 m^2/g, 0.12 cm^3/g). It was confirmed that the recovered material exhibited a mesoporous structure, with an average pore diameter of 4.4 nm (Figure S2). Such properties are considered to be exceptionally important in catalysis, as they can reduce transfer and diffusion limitations and increase accessibility to active sites.


Figure 1. a) XRD patterns of MFI silicate-1 samples at various times of crystallization at 180 °C; b) - e) TEM images of MFI silicate-1 samples after 0, 4, 8, and 12 h of crystallization at 180 °C, respectively; f) 29Si MAS NMR spectra of the MFI silicate-1 at various times of crystallization 180 °C.

In-situ DRIFT spectroscopy was subsequently utilized to monitor the solid-phase structural transformation of the mixture of SiO_2 and $C_{12}H_{28}NF$ during the crystallization process. To ensure that observations were not attributed to changes in the structure of the reagents independently, two control experiments were conducted which involved heating the two reagents separately. For each of these experiments, the reagents were added into the DRIFT cell and heated from 20 °C to 180 °C, where the temperature was maintained for a set time. When SiO_2 gel was run independently, the structural properties remained almost unchanged (Figure S3). Similar observations were also made by monitoring the $(CH_3CH_2CH_2)_4NF$ (Figure S4). Three significant vibrational peaks of ν(C-H) at *ca.* 2845-2975 cm^{-1}, characteristic of vibrations in -CH_3, -CH_2 and -CH_2 groups of $CH_3CH_2CH_2)_4NF$,[23] were used to monitor whether any changes in this material occurred. However, no significant changes in intensity were observed during this stage of the procedure. From these observations, it is evident that the SiO_2 gel and $(CH_3CH_2CH_2)_4NF$ are stable when exposed to the crystallization conditions independently.

Following these control experiments, a mixture of SiO_2 and $(CH_3CH_2CH_2)_4NF$ was combined in the DRIFT cell and exposed to the same heating procedure. As shown in Figure 2a, three peaks at *ca.* 2880 cm^{-1} which are characteristic of C-H stretches were assigned to the $(CH_3CH_2CH_2)_4N^+$, while the peaks at 1470 cm^{-1} and 1380 cm^{-1} were attributed to the in-plane bending vibrations of δ_{as}(C-H) and δ_s(C-H), respectively.[23] A notable change is observed after just 10 minutes (60 °C) of heating (Figure 2a & Figure S6). Prior to this 10-minute mark, the peaks characteristic of the C-H stretching vibrations ν(C-H) are clearly visible, located at *ca.* 2845-2975 cm^{-1} and are consistent with those observed in the

spectrum of $C_{12}H_{28}NF$ (Figure S4). This indicates that the $C_{12}H_{28}N^+$ remained unchanged during the first 10 minutes of analysis (20-60 °C), after which point it rapidly interacts with SiO_2 species. This is evidenced by a significant reduction in the intensity of the C-H stretching vibrations (Figure 2a). As the temperature of the DRIFT cell reaches and is maintained at 180 °C, changes in the spectra are reported over time in Figure 2b (from 1 to 12 h). The spectrum of the mixture after heating for 8 h contains a peak at *ca.* 1125 cm^{-1}, which is characteristic of an asymmetric ν_{as}(Si-O) stretch[20, 21] and evidences that Si-O bond formation has occurred. After 12 h, the intensity of the peak at 1125 cm^{-1} increases further and two new peaks at 1167 and 1200 cm^{-1} also emerge. These two additional peaks can be assigned to the tetrahedral asymmetric stretching vibration of ν_{as}(SiO_4),[20-22] evidencing that after 12 h of reaction, the formation of tetrahedral skeleton is achieved. XRD patterns of this sample after 12 h confirmed that the diffractions characteristic of MFI were observable in Figure S7a. Additional vibrations at 465 cm^{-1} and 544 cm^{-1} are also observed after 12 h of reaction, which are characteristic of double penta-rings of MFI zeolite (Figure S7b).[19]

Synthesis of ZSM-5 with Si/Al ratio of 18-∞.

Given that the MFI silicalite-1 has no acidity, it has limited catalytic applications. Aluminosilicate ZSM-5 zeolite on the other hand consists of acid sites; the strength and abundance of which can be tailored. For this reason and its unique pore structure, ZSM-5 zeolites are considered to be one of the most important zeolites from an industrial perspective. To establish whether the novel methodology invoked for the synthesis of MFI silicalite-1 zeolite could be used for the synthesis of ZSM-5, some new experiments were conducted.

For this, NaAlO$_2$ was added to the mixture of SiO$_2$ and (CH$_3$CH$_2$CH$_2$)$_4$NF, ground together and sealed in an autoclave. Once again, the temperature of the autoclave was increased steadily to 180 °C, where it was maintained for up to 48 h. The XRF measurements confirm that weight ratio of Na accounts for ca. 0.059 and 0.001 present in the final pre-synthesized from NaAlO$_2$ and (NH$_4$)$_3$AlF$_6$, respectively. The corresponding diffraction peaks and changes in crystallinity for the samples at different reaction times are displayed in Figures 3a and 3b, respectively. Diffraction peaks characteristic of ZSM-5 zeolite appear after 8 h of reaction, though the crystallinity at this stage is quite low (< 60% in Figure 3b). The crystallinity of the sample reached a maximum after 24 h of reaction, after which no further notable changes in crystallinity was observed. As evidenced, the addition of an Al precursor requires a longer crystallization time compared to the synthesis of MFI zeolite (12 h).
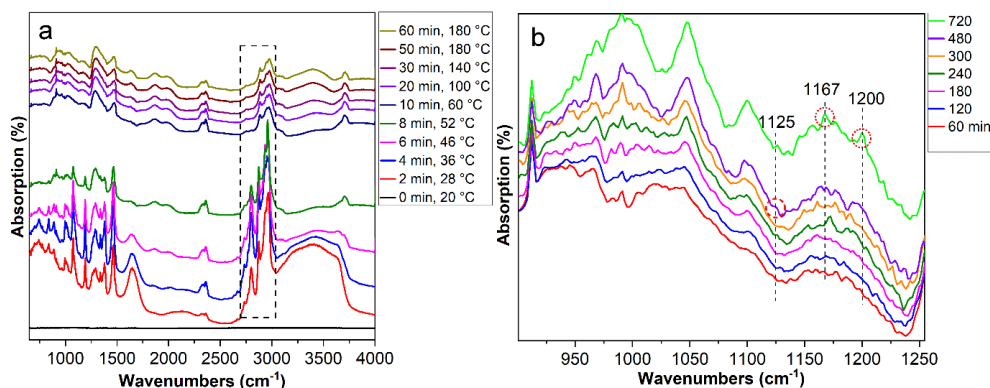

Figure 2. In-situ DRIFT spectra of the MFI silicate-1 sample from SiO$_2$ and C$_{12}$H$_{28}$NF in an in-situ pool at atmospheric pressure at the rate of 4 °C/min from 20 °C (0 min) to 180 °C, and then keep at 180 °C until 720 min. More details see Figure S5-S6 and Table S1.

The ratio of Si/Al is a very important parameter of ZSM-5 zeolites, as this is what ultimately dictates the concentration of acid sites that are present in the material. As such, it was quite significant to assess what concentrations of Al can be obtained in ZSM-5 materials through the crystallization process. Surprisingly, it was determined that ZSM-5 zeolites with a wide range of Si/Al ratios could be prepared in this way; a ZSM-5 zeolite with a Si/Al ratio as low as 5 was produced. It is important to note that the Si/Al ratios discussed herein, are calculated theoretically from the quantities of each in the raw feed (SiO$_2$ / NaAlO$_2$). This methodology is applied throughout this work, unless stated otherwise. Figure 3c contains XRD patterns for synthesized ZSM-5 zeolites with differing Si/Al ratios, all of which consist of characteristic MFI diffraction peaks. The crystallinity of these materials does however decrease significantly as the Si/Al ratio was reduced.

It is well established that the Al precursors play an important role in the synthesis of aluminosilicate zeolites, and determine the scope of the obtainable Si/Al ratios. To obtain ZSM-5 materials which could have a wide range of Si/Al ratios, it was important to establish how other Al precursors influenced the crystallization process. For this a series of additional crystallization experiments were conducted using alternative aluminum precursors to NaAlO$_2$, which included aluminum isopropoxide [(C$_3$H$_7$O)$_3$Al], aluminum sec-butoxide [(C$_4$H$_9$O)$_3$Al]), aluminum chloride (AlCl$_3$·6H$_2$O), ammonium fluoroaluminate [(NH$_4$)$_3$AlF] and aluminum sulfate [Al$_2$(SO$_4$)$_3$·18H$_2$O]). Once again, the quantity of aluminum precursor was varied to establish how this influenced the crystallization process. Each crystallization experiment was conducted using the same procedure reported previously; precursors were added to an autoclave which was steadily heated to 180 °C and the temperature maintained for up to 48 h. Each of the resultant material was probed by XRD (Figure S8), and the obtainable Si/Al ratios using the different Al precursors are outlined in Figure 4. The use of NaAlO$_2$ and (NH$_4$)$_3$AlF$_6$ allowed for the synthesis of ZSM-5 materials with the widest range of Si/Al ratios, from as low as 18 to infinity. Whilst the (C$_4$H$_9$O)$_3$Al and (C$_3$H$_7$O)$_3$Al precursors were also effective (Si/Al > ~40), materials containing higher concentrations of Al were not obtainable. It was also established that some inorganic Al substrates such as [Al$_2$(SO$_4$)$_3$·18H$_2$O] can also be used to produce Al-containing ZSM-5 (Si/Al = 57). When AlCl$_3$·6H$_2$O was trialed, no crystallization was observed and no zeolitic material was obtained (Figure S8c). The logical deduction is likely that this crystallization suppression is attributed to the Cl$^-$ anions occupying positions typically filled by F$^-$ anions, which ultimately inhibits the key role of F$^-$ during solid-phase crystallization. Besides, it is worth mentioning that a trace amount of water embodied in the raw materials is significant for crystallization, although no additional water was added into synthesis. This is consistent with the results reported by Xiao's group.[11-13, 15, 16] The underlying roles of water during crystallization is still obscure and under investigation.
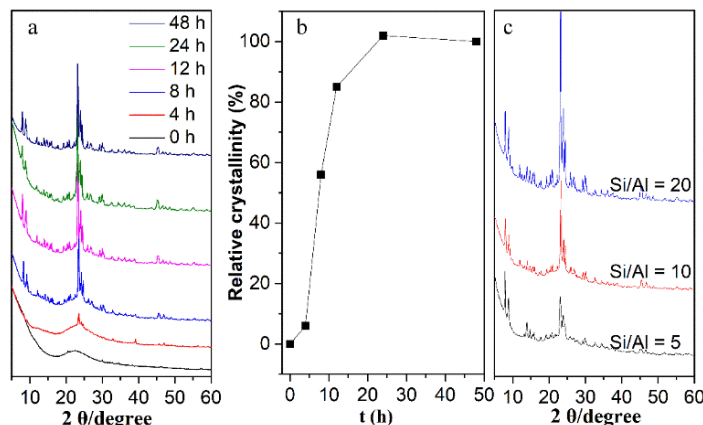
Figure 3. (a) XRD patterns of ZSM-5 samples with different crystallization time at 180 °C using SiO$_2$, (CH$_3$CH$_2$CH$_2$)$_4$NF and NaAlO$_2$ as raw materials. (b) Relative crystallinity of ZSM-5 samples at 0, 4, 8, 12, 24, 48 h (The crystallinity of zeolite at 180 °C was denoted as 100%) (c) XRD patterns of ZSM-5 zeolite with different Si/Al ratios.
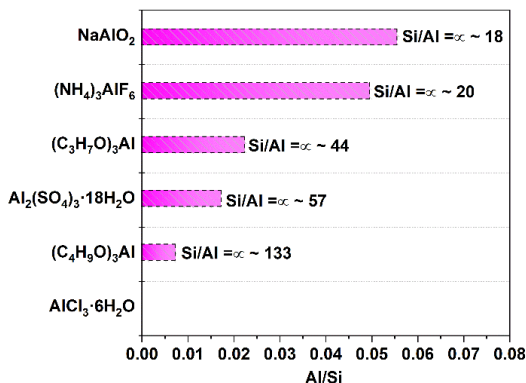
Figure 4. The Si/Al ratios of ZSM-5 synthesized using different Al sources in the seed-free and solvent-free method. The synthetic condition is that an Al precursor, mixed with SiO$_2$ and C$_{12}$H$_{28}$NF, was ground and sealed at 180 °C for 48 h. The crystallinity of ZSM-5 prepared by NaAlO$_2$ (180 °C, 48 h) was used as a reference (100%). When the crystallinity of a zeolite synthesized by a certain Si/Al ratio exceeded 80%, it was considered that the crystalline zeolite was successfully obtained at this Si/Al ratio.

The proposed mechanism of crystallization

A series of additional experiments were subsequently conducted in order to derive a greater understanding of the mechanism of crystallization.[24] C$_{12}$H$_{28}$NBr and NH$_4$F were used as substitutes for C$_{12}$H$_{28}$NF to run some control experiments. For these experiments, mixtures of SiO$_2$, C$_{12}$H$_{28}$NBr, and NH$_4$F were ground, sealed into an autoclave and maintained at 180 °C for 15 h. The corresponding XRD patterns for the recovered materials after 15 h are displayed in Figure S9. Interestingly, crystalline MFI zeolite was not obtained; only a broad peak of amorphous SiO$_2$ and diffraction peaks characteristic of NH$_4$SiF$_6$ were observable in the XRD pattern of the recovered material (Figure S9). This indicates that the F$^-$ anions must be in close proximity to the C$_{12}$H$_{28}$N$^+$ cation to facilitate crystallization. The roles of C$_{12}$H$_{28}$N$^+$ have been being investigated and are acknowledged to be effective templates for the synthesis of zeolites with an MFI framework in hydrothermal synthesis.[25, 26] C$_{12}$H$_{28}$N$^+$ is embedded into the silicate network, forming C$_{12}$H$_{28}$N$^+$-silicate clathrates; amorphous colloidal particles which are several nanometers in diameter. They are the primary building blocks of ZSM-5, whose conformation and confinement resemble their positions in channel intersections of

crystalline C$_{12}$H$_{28}$N$^+$-ZSM-5.[27] When compared with the hydrothermal synthesis procedure, F$^-$ anions in this solvent-free synthesis were also found to play a very important role in this synthesis methodology.

^{29}Si, ^{27}Al and ^{19}F MAS NMR experiments were subsequently performed in order to assess how the chemical environment evolves during the ZSM-5 crystallization process when the standard procedure and reagents were employed.[28, 29] ^{29}Si NMR spectra corresponding to the ZSM-5 sample after various lengths of crystallization (0—24 h) are displayed in Figure S10-S12. The peak intensity increases and becomes narrower as the reaction time was extended from 0 h to 12 h, indicating that the material becomes more crystalline over time.[16] The ^{19}F MAS NMR spectrum of these synthesized samples is displayed in Figure 5a. The intense resonance centered at *ca.* -119 ppm was ascribed to F$^-$ species balancing the charge of C$_{12}$H$_{28}$N$^+$ quaternary cations within pores.[30] This phenomenon was observed throughout the crystallization process. Two additional resonances are also observed at *ca.* -65 ppm and *ca.* -80 ppm, which can be attributed to F$^-$ anions occupying positions within the cages [4^{1}5^{2}6^2] of zeolitic framework[31-33] and interacting with penta-coordinated [SiFO$_4$]$^-$ species,[33-35] respectively. The spatially coordinated conformations of these species are illustrated in Figure 5d. Interestingly, these peaks did not emerge until after 4 h of reaction and appeared to become more prominent as the crystallization time was extended. This indicates that F$^-$ anions migrate into the zeolite cage, which in turn facilitates the formation of Si-O tetrahedrons in the zeolitic framework.

Additional high-field signals at *ca.* -178 ppm and -191 ppm were also observed. We consider these to be attributed to the existence of Na$^+$ in F-bearing aluminosilicate species. The former can be assigned to the F atoms in tetrahedral Al species, such as [AlF$_2$O$_2$]$^-$···Na$^+$; based on previous reports.[36, 37] This signal first emerges after 8 h of crystallization, but continues to increase in intensity over time. The strong ^{19}F signal at -191 ppm could evidence the formation of hexa-coordinated ~~[AlF$_x$(OSi(OH)$_3$)$_{6-x}$]$^{3-}$—Na$^+$~~ and penta-coordinated ~~[AlF$_x$(OSi(OH)$_3$)$_{5-x}$]$^{2-}$—Na$^+$~~ structures. Previous studies have suggested that the former is unstable and rapidly decomposes to the corresponding penta-coordinated Al species upon formation.[36, 38] This 'F-Al-O-Si' signal also appears to increase in intensity as the crystallization process proceeds. It can therefore be proposed that the formation of the zeo-

5

litic framework is instigated through the migration of F⁻ anions which was in coordination with $C_{12}H_{28}N^+$ to produce "F-Al-O-Si" containing species.

Similar conclusions can also be drawn from inspection of the ^{27}Al NMR spectrum (Figure 5b). The signal at *ca.* 79 ppm can be assigned to anionic $Al(OH)_4^-$ species in the Al-containing raw materials.[39, 40] The additional resonances observed at *ca.* 52 ppm and 25 ppm are attributed to tetrahedral $[AlO_4]^-$ and penta-coordinated $[AlO_5]^{2-}$ anions, respectively. Interestingly, the width of the signal at 52 ppm gradually narrowed and became more defined as the crystallization time was increased, indicating that the quantity of $[AlO_4]^-$ present increases over time. However, the other signal at *ca.* 25 ppm did not appear until after 8 h of crystallization, which suggests that it is indicative of penta-coordinated Al species $[AlF_x(OSi(OH)_3)_{5-x}]^{2-}\cdots Na^+$. After this signal first appears, it too continues to increase in intensity over time. Peaks at *ca.* 0 ~ 7 ppm were also observed and can be assigned to hexa-coordinated Al in $[AlF_x(OSi(OH)_3)_{6-x}]^{3-}\cdots Na^+$ species. We therefore propose that the formation of "F-Al-O-Si" species, leads to the construction of tetrahedral $[AlO_4]^-$ units. The small amounts of

F⁻ retained in zeolite can be removed by pyrolydrolytic extraction techniques, which are commonly employed to remove trace quantities of F⁻ from glasses, rocks and minerals and raw materials or products in some industrial processes.[41, 42] Interactions between F and Al atoms in the various intermediates species formed during the crystallization process were further studied by a 2D [19]F-[27]Al heteronuclear correlation (HETCOR) NMR technique (Figure 5c).[39, 43] At the initial stage of the crystallization process no correlation was detected, as shown in Figure 5c (t = 0 h). However, when the crystallization time was extended to 4 h, a very weak correlation peak at *ca.* (0, -189) ppm was observed, indicative of the incipient transfer of F⁻ ions from the $C_{12}H_{28}N^+F^-$ molecules, in the formation of the 'F-Al-O-Si' species. As the crystallization time was increased (t = 8 h), this peak increased to *ca.* (0-7, -191) ppm. This further evidences that the 'F-Al-O-Si' species, such as $[AlF_x(OSi(OH)_3)_{6-x}]^{3-}\cdots Na^+$ and $[AlF_x(OSi(OH)_3)_{5-x}]^{2-}\cdots Na^+$, play a crucial role in the crystallization process. The data acquired from the 2D NMR experiments are consistent with the 1D ^{27}Al and ^{19}F NMR spectra and provide solid experimental evidence of the importance of the 'F-Al-O-Si' species in the crystallization process.

Figure 5. (a) ^{19}F and (b) ^{27}Al MAS NMR spectra of ZSM-5 zeolites crystallized for 0, 4, 8, and 12 h. (c) 2D [19]F-[27]Al HETCOR MAS
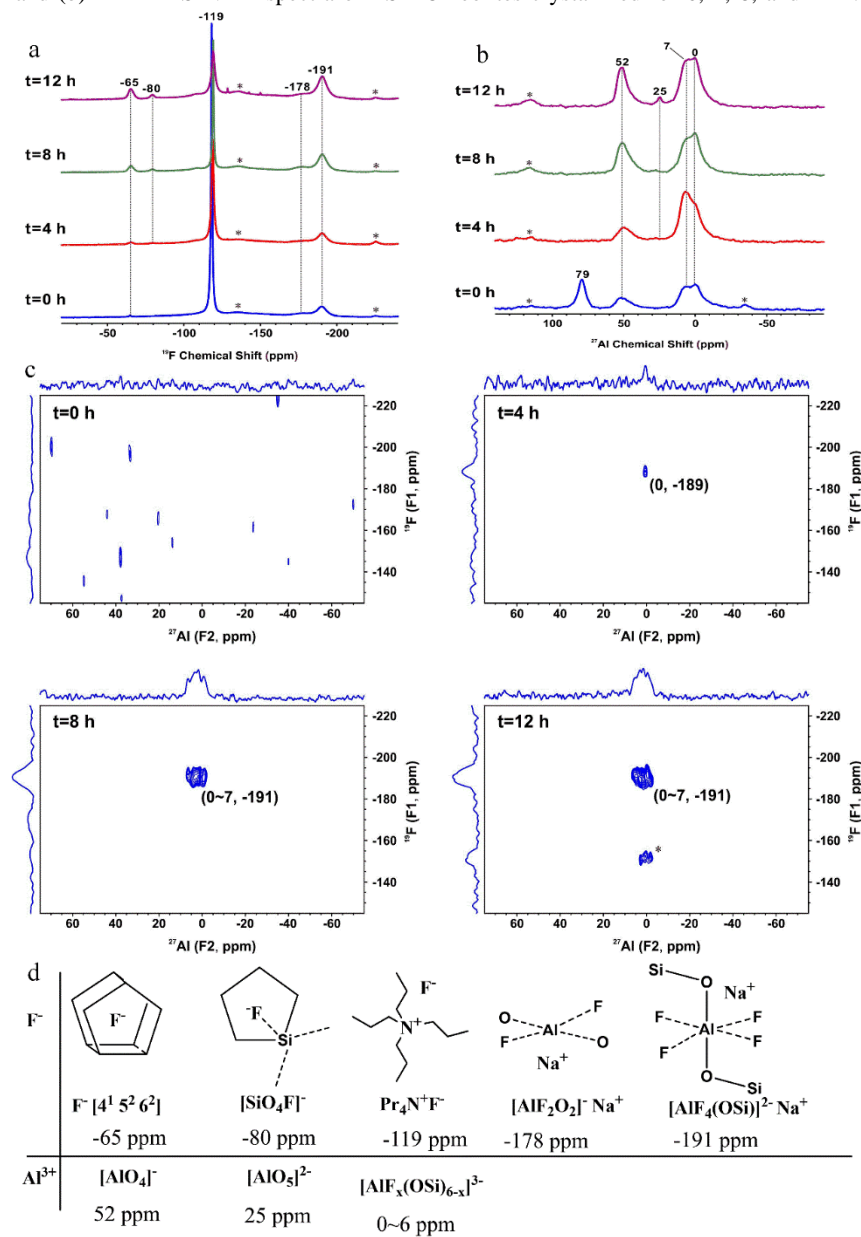
NMR spectra of ZSM-5 zeolites crystallized for 0, 4, 8, and 12 h. (d) Possible spatially coordinated conformations of fluoride anions and aluminum ions during crystallization.

The textural properties, acidity and performance as a catalyst support

The textural properties of the materials formed as a function of crystallization time (0 ~ 48 h) were also investigated, using SiO_2, $C_{12}H_{28}NF$ and $NaAlO_2$ as raw materials and the autoclave temperature fixed at 180 °C. Each of the materials exhibited characteristic IV-type isotherms, whatever the timing, as shown in Figure S13. The initial sample mixture (t = 0 h) presented a hysteresis loop of H2 and is characteristic of porous SiO_2 gel. As the time increased (t > 4 h) the hysteresis loop became H3 in character, which typically indicates that slit apertures are present, but can also be derived from sheet particles.[44] We propose that this evidences the formation of the colloidal aggregations during crystallization process, as previously depicted in Figure 1. When the final material after 48 h of crystallization was calcined, it exhibited a H4-type hysteresis loop, which is often observed in microporous materials like activated carbon, etc. This result is consistent with that of the commercial ZSM-5 zeolites. It demonstrates this ZSM-5 material consists of both meso- and micropores, which aligns with corresponding industrial ZSM-5 sample. The BET surface area, microporous surface area, pore volume and pore diameters for each of the samples are displayed in Table S2.

Aluminosilicate ZSM-5 typically consists of both Brønsted (B) and Lewis (L) acid sites,[45] which arise from an imbalance between the valence states of Si^{4+} and Al^{3+} and the unsaturated coordination of Al.[46, 47] Pyridine-FTIR spectroscopy was used to monitor the acidic sites of ZSM-5 materials (Si/Al = 53) synthesized from aluminum isopropoxide (Figure S14A-C). In a typical experiment, pyridine vapor was passed over the catalyst at 50 °C for a fixed period and subsequently heated to 200 °C under N_2, to ensure that any physisorbed pyridine was desorbed and the spectrum was stable. The peaks at 1540, 1490, 1450 cm^{-1} are characteristic of B, B+L, and L acidic sites, respectively.[48, 49] The peak at 1595 cm^{-1}, is typically attributed to strong L acid sites[50], the broad peak at 1620 cm^{-1} is typically attributed to a bending mode of physisorbed water.[51] Even upon sequential heating to 300 °C, these peaks are still distinguishable, although a notable reduction in the associated intensity is observed. The pyridine-FTIR spectra of the as-prepared ZSM-5 sample with higher Si/Al ratios of 133, are also presented in Figure S15. It presented a similar trend with that zeolite sample (Si/Al = 53), but a notable reduced peak intensity. In addition, the spectra of the ZSM-5 prepared using $NaAlO_2$ as the precursor was shown in Figure S16. No pyridine-adsorption peak can be observed in this Na-type zeolite.

The catalytic viability of the synthesized ZSM-5 zeolites with different Si/Al ratios was accessed.[52] The materials were used as supports for Ru nanoparticles and tested for the aqueous phase hydrogenation of levulinic acid at mild temperature. As shown in Figure 6, after loaded the Ru component, Ru/ZSM-5 (Si/Al = 133) catalyst gave a better activity than Ru/silicalite-1 (Si/Al = ∞). It gave an 85% yield of γ-valerolactone at 100% conversion of levulinic acid at 70 °C, which is close to the performance of a commercial ZSM-5 supported Ru catalyst. These catalysts also catalyzed hydrogenation of glucose to hexitol at water. The Ru/silicalite-1 catalyst presented almost 100% yield of hexitol, which has a similar result to the commercial one. Evidently, the zeolitic materials synthesized in this study exhibited an excellent performance as catalyst support for Ru nanoparticles in two different hydrogenation reactions.
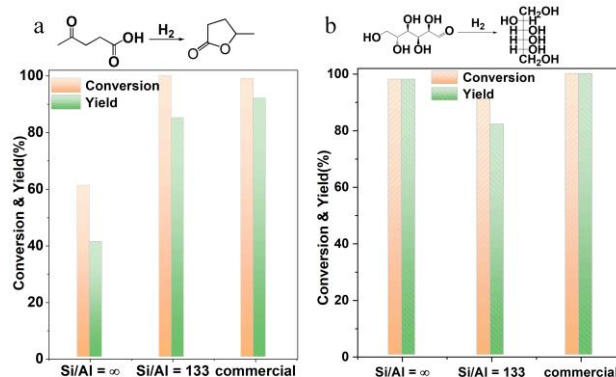
Figure 6. Catalytic performances of Ru/ZSM-5 zeolite catalysts with as-prepared ZSM-5 and commercial ZSM-5 zeolites. Reaction conditions: (a) 70 °C for 6 h in water at H_2 for hydrogenation of levulinic acid. (b) 120 °C for 2.5 h in water at H_2 for hydrogenation of glucose.

CONCLUSIONS

ZSM-5 with tuneable Si/Al ratios were successfully synthesized using a facile, green and efficient solvent-free method with only three starting reagents and without seed crystals. The Al precursor used in the experimental procedure is very important and can significantly influence the ratio of Si/Al in the final ZSM-5 material. Investigation into the mechanism of crystallization confirmed that the F⁻ anion must be in close proximity to the $C_{12}H_{28}N^+$ cation for the ZSM-5 crystallization to occur. It was also determined that the anionic F⁻ coordinates with Al^{3+} species, forming hexa-coordinated "F-Al-O-Si" species, which we consider drives the formation of the tetrahedral units of zeolitic framework. We hope that identifying the important role of the anionic F⁻ in this procedure will pave the way for the rational design of other structure-directing agents for the synthesis of zeolites.

ASSOCIATED CONTENT

Supporting Information

The Supporting Information is available free of charge on the RSC Publications website.

Figure S1 - S16 and Table S1 - S2 are provided as a Source Data file. (PDF)

AUTHOR INFORMATION

Corresponding Author

*czhang@ciac.ac.cn
*hutch@cardiff.ac.uk

Author Contributions

All authors discussed the results and commented on the manuscript.

REFERENCES

1. M. Dusselier, P. Van Wouwe, A. Dewaele, P. A. Jacobs and B. F. Sels, *Science*, 2015, **349**, 78-80.
2. M. Moliner, C. Martínez and A. Corma *Angewandte Chemie International Edition*, 2015, **54**, 3560-3579.
3. T. Degnan, G. Chitnis and P. H. Schipper, *Microporous and Mesoporous materials*, 2000, **35**, 245-252.
4. E. R. Cooper, C. D. Andrews, P. S. Wheatley, P. B. Webb, P. Wormald and R. E. Morris, *Nature*, 2004, **430**, 1012.
5. E. R. Parnham and R. E. Morris, *Accounts of chemical research*, 2007, **40**, 1005-1013.
6. M. Matsukata, N. Nishiyama and K. Ueyama, *Microporous materials*, 1996, **7**, 109-117.
7. Q. Wu, X. Meng, X. Gao and F.-S. Xiao, *Accounts of chemical research*, 2018, **51**, 1396-1403.
8. U. Deforth, K. K. Unger and F. Schüth, *Microporous Materials*, 1997, **9**, 287-290.
9. W. Xu, J. Dong, J. Li, J. Li and F. Wu, *Journal of the Chemical Society, Chemical Communications*, 1990, 755-756.
10. R. Althoff, R. Althoff, K. Unger, K. Unger, F. Schüth and F. Schueth, *Microporous Materials*, 1994, **2**, 557-562.
11. L. Ren, Q. Wu, C. Yang, L. Zhu, C. Li, P. Zhang, H. Zhang, X. Meng and F.-S. Xiao, *Journal of the American Chemical Society*, 2012, **134**, 15173-15176.
12. Y. Y. Jin, Q. Sun, G. D. Qi, C. G. Yang, J. Xu, F. Chen, X. J. Meng, F. Deng and F. S. Xiao, *Angewandte Chemie-International Edition*, 2013, **52**, 9172-9175.
13. Q. Wu, X. Wang, G. Qi, Q. Guo, S. Pan, X. Meng, J. Xu, F. Deng, F. Fan, Z. Feng, C. Li, S. Maurer, U. Müller and F.-S. Xiao, *Journal of the American Chemical Society*, 2014, **136**, 4019-4025.
14. M. H. Nada, E. G. Gillan and S. C. Larsen, *Microporous and Mesoporous Materials*, 2019, **276**, 23-28.
15. Q. Wu, L. Zhu, Y. Chu, X. Liu, C. Zhang, J. Zhang, H. Xu, J. Xu, F. Deng, Z. Feng, X. Meng and F.-S. Xiao, *Angewandte Chemie International Edition*, 2019, **58**, 12138-12142.
16. Q. Wu, X. Liu, L. Zhu, L. Ding, P. Gao, X. Wang, S. Pan, C. Bian, X. Meng, J. Xu, F. Deng, S. Maurer, U. Müller and F.-S. Xiao, *Journal of the American Chemical Society*, 2015, **137**, 1052-1055.
17. X. Lu, Y. Yang, J. Zhang, Y. Yan and Z. Wang, *Journal of the American Chemical Society*, 2019, **141**, 2916-2919.
18. D. Wu, X. Yu, X. Chen, G. Yu, K. Zhang, M. Qiu, W. Xue, C. Yang, Z. Liu and Y. Sun, *ChemSusChem*, 2019, DOI: 10.1002/cssc.201900663, 1-8.
19. S. L. Burkett and M. E. Davis, *Journal of Physical Chemistry*, 1994, **98**, 4647-4653.
20. Y. Tao, H. Kanoh and K. Kaneko, *Journal of the American Chemical Society*, 2003, **125**, 6044-6045.
21. N. Chu, J. Yang, C. Li, J. Cui, Q. Zhao, X. Yin, J. Lu and J. Wang, *Microporous and Mesoporous Materials*, 2009, **118**, 169-175.
22. X. Yang, L. Huang, G. Du and X. Lu, *Journal of Porous Materials*, 2017, **24**, 881-886.
23. K. F. M. G. J. Scholle, W. S. Veeman, P. Frenken and G. P. M. van der Velden, *Applied Catalysis*, 1985, **17**, 233-259.
24. M. B. Park, Y. Lee, A. Zheng, F.-S. Xiao, C. P. Nicholas, G. J. Lewis and S. B. Hong, *Journal of the American Chemical Society*, 2013, **135**, 2248-2255.
25. Peter-Paul E. A. de Moor, a. Theo P. M. Beelen and R. A. v. Santen, 1999, DOI: 10.1021/JP982553Q.
26. J. B. Nagy, G. Debras, E. G. Derouane, Z. Gabelica, N. Blom, P. K. Dutta, D. C. Shieh and M. Puri, 1992.
27. P. C. M. M. Magusin, V. E. Zorin, A. Aerts, C. J. Y. Houssin, A. L. Yakovlev, C. E. A. Kirschhock, J. A. Martens and R. A. van Santen, *The Journal of Physical Chemistry B*, 2005, **109**, 22767-22774.
28. M. Haouas, *Materials*, 2018, **11**, 1416.
29. J. D. Epping and B. F. Chmelka, *Current Opinion in Colloid & Interface Science*, 2006, **11**, 81-117.
30. R. D. Gougeon, E. B. Brouwer, P. R. Bodart, L. Delmotte, C. Marichal, J.-M. Chézeau and R. K. Harris, *The Journal of Physical Chemistry B*, 2001, **105**, 12249-12256.
31. C. A. Fyfe, D. H. Brouwer, A. R. Lewis and J.-M. Chézeau, *Journal of the American Chemical Society*, 2001, **123**, 6882-6891.
32. X. Liu, U. Ravon and A. Tuel, *Angewandte Chemie International Edition*, 2011, **50**, 5900-5903.
33. L. A. Villaescusa, I. Bull, P. S. Wheatley, P. Lightfoot and R. E. Morris, *Journal of Materials Chemistry*, 2003, **13**, 1978-1982.
34. H. Koller, A. Wölker, L. A. Villaescusa, M. J. Díaz-Cabañas, S. Valencia and M. A. Camblor, *Journal of the American Chemical Society*, 1999, **121**, 3368-3376.
35. P. J. Chupas, D. R. Corbin, V. N. M. Rao, J. C. Hanson and C. P. Grey, *The Journal of Physical Chemistry B*, 2003, **107**, 8327-8336.
36. Y. Liu and J. Tossell, *The Journal of Physical Chemistry B*, 2003, **107**, 11280-11289.
37. J. Tossell, *Annual Reports on NMR Spectroscopy*, 2008, **64**, 1-19.
38. J. L. Guth, L. Delmonte, M. Soulard, B. Brunard, J. F. Joly and D. Espinat, *Zeolites*, 1992, **12**, 929-935.
39. Z. Miladinović, J. Zakrzewska, B. Kovačević and G. Bačić, *Materials Chemistry and Physics*, 2007, **104**, 384-389.
40. X. Yi, K. Liu, W. Chen, J. Li, S. Xu, C. Li, Y. Xiao, H. Liu, X. Guo, S.-B. Liu and A. Zheng, *Journal of the American Chemical Society*, 2018, **140**, 10764-10774.
41. A. Pandey, A. Kelkar, R. K. Singhal, C. Baghra, A. Prakash, M. Afzal and J. P. Panakkal, *Journal of Radioanalytical and Nuclear Chemistry*, 2012, **293**, 743-749.
42. R. L. Clements, G. A. Sergeant and P. J. Webb, *Analyst*, 1971, **96**, 51-54.
43. X. Liu, Y. Chu, Q. Wang, W. Wang, C. Wang, J. Xu and F. Deng, *Solid State Nuclear Magnetic Resonance*, 2017, **87**, 1-9.
44. R. Xu, W. Pang, J. Yu, Q. Huo and J. Chen, *Chemistry of zeolites and related porous materials: synthesis and structure*, John Wiley & Sons, 2009.
45. S. Li, A. Zheng, Y. Su, H. Zhang, L. Chen, J. Yang, C. Ye and F. Deng, *Journal of the American Chemical Society*, 2007, **129**, 11161-11171.
46. A. Zheng, S.-J. Huang, S.-B. Liu and F. Deng, *Physical Chemistry Chemical Physics*, 2011, **13**, 14889-14901.
47. A. Zheng, S. Li, S.-B. Liu and F. Deng, *Accounts of chemical research*, 2016, **49**, 655-663.
48. Y. Wang, X. Guo, C. Zhang, F. Song, X. Wang, H.-o. Liu, X. Xu, C. Song, W. Zhang, X. Liu, X. Han and X. Bao, *Catalysis Letters*, 2006, **107**, 209-214.
49. J. Liu, X. Li, Q. Zhao, D. Zhang and P. Ndokoye, *Journal of Molecular Catalysis A: Chemical*, 2013, **378**, 115-123.
50. H. Zhou, M. Ge, S. Wu, B. Ye and Y. Su, *Fuel*, 2018, **220**, 330-338.

51.   K. Nakajima, J. Hirata, M. Kim, N. K. Gupta, T. Murayama, A. Yoshida, N. Hiyoshi, A. Fukuoka and W. Ueda, *ACS Catalysis*, 2018, **8**, 283-290.

52.   J. Xu, Q. Wang and F. Deng, *Accounts of Chemical Research*, 2019, **52**, 2179-2189.

Graphical Abstract
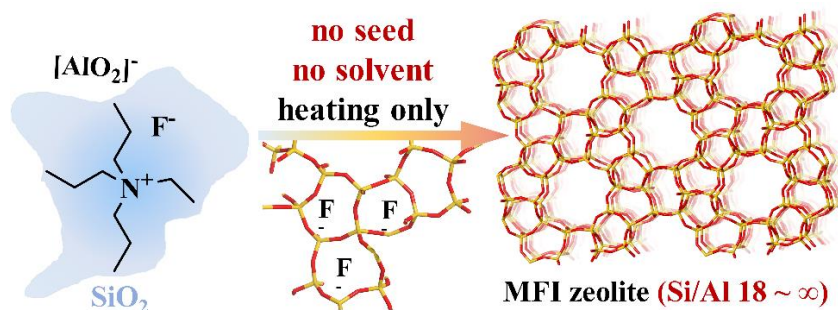
Novel seed-free and solvent-free synthesis of MFI zeolites with tuneable Si/Al ratios (18-∞) was achieved herein. The option of the Al precursor used can significantly influence the ratio of Si/Al in the final ZSM-5. The key role of F^- was that forming 6-coordinated "F-Al-O-Si" species drove the formation of tetrahedral units in the zeolitic framework during crystallization.